RSC Advances

ROYAL SOCIETY OF CHEMISTRY

www.rsc.org/advances

RSC Advances

RSCPublishing

ARTICLE

Electrochemical fabrication of $Ni(OH)_2$/Ni 3D porous composite films as integrated capacitive electrodes

Cite this: DOI: 10.1039/xoxxoooooox

Received ooth January 2012,
Accepted ooth January 2012

DOI: 10.1039/xoxxoooooox

www.rsc.org/

Hong Jiang[a,b], Ying Guo[a], Tao Wang[a], Peng-Li Zhu[a], Shuhui Yu[a], Yan Yu[b], Xian-Zhu Fu[a,*], Rong Sun[a,*], Ching-Ping Wong[c,d]

$Ni(OH)_2$ coated on Ni porous films are facilely fabricated by anode oxidation of 3D hierarchical porous Ni films which prepared through a hydrogen bubble template electro-deposition method. The highly porous nickel films function as effective 3D conductive network current collectors and scaffolds to in-situ form thin layer of $Ni(OH)_2$ active material. The electrochemical capacitive performances are investigated by cyclic voltammetry (CV) and galvanostatic charge-discharge technique in 6 M KOH electrolyte. The 3D porous $Ni(OH)_2$/Ni integrated electrodes demonstrate a much higher specific capacity of 828 mF/cm^2 than 126 mF/cm^2 for the smooth $Ni(OH)_2$/Ni electrode at a current density of 10 mA/cm^2. The 3D porous $Ni(OH)_2$/Ni integrated electrodes also display a good capacity retention of 95% after 1000 cycles. The superior capacitive properties of 3D porous $Ni(OH)_2$/Ni electrodes might result from the thin layer $Ni(OH)_2$ active materials in-situ formed on the highly 3D porous Ni metallic current collector with large surface area, low contact resistance between $Ni(OH)_2$ active material and Ni current collector, and fast electron/ion conduction.

Introduction

Supercapacitors, also named as electrochemical capacitors, are considered as promising energy storage devices due to the advantages including high power density, long cycle life, fast charge-discharge process, and lower maintenance cost.[1-4] Electrode material with high performance and low cost is a key for the practical application of supercapacitors. Transition metal oxides/hydroxides have attracted increasing attention as capacitive electrode materials in recent years owing to their large specific capacitance.[5-7] Among them, $Ni(OH)_2$ (nickel hydroxide) has been widely used as the positive electrode material of nickel-based secondary batteries for many years.[8] $Ni(OH)_2$ is also identified as one of the most promising electrode materials for supercapacitors because of its high theoretical specific capacitance, easy synthesis, low cost, environmental compatibility, and good rate capability.[9-11] Unfortunately, $Ni(OH)_2$ still suffers from lower capacity especially at high rate compared to the theoretical value owing to its too poorly conducting to support fast electron transport.[12] Furthermore, the traditional strategy to fabricate electrodes used conductive agent, polymer binder and active materials to coat on the nickel foam, which would decrease the contact area of active material to the current collector and electrolyte solution, hamper the electron/ion transport rate, increase the total electrode mass and decrease the capacity.[13,14]

Growth of $Ni(OH)_2$ directly on the conductive substrates is an effective method to address the above problems. Lots of conductive materials have been developed to support $Ni(OH)_2$ active materials, such as carbon nanotubes,[15] graphene nanosheets,[16] 3D graphene foams,[17] mesoporous carbon,[18] graphite sheets,[19] graphite foam,[20] and Ni foams.[5-7] These conductive substrate materials can improve the electrical conductivity of the composites and shorten the electron and ion diffusion pathways thus to efficiently utilize the $Ni(OH)_2$ active materials and improve the electrochemical performance.[21] Especially, highly conductive 3D continuous porous matrixes could provide high surface area for loading $Ni(OH)_2$ active materials, greatly facilitate the fast electron transport from $Ni(OH)_2$ active materials to the current collectors. Moreover, it would not need conductive agent and polymer binder for the integrated electrodes of coating of $Ni(OH)_2$ active materials on the conductive current collector.[22] 3D porous metal films prepared by a hydrogen bubble template have attracted much interest for their high surface area, open porous structures and facile fabrication.[23-28] But there are few reports about hydrogen bubble template to prepare 3D porous metallic current collectors supported capacitive materials, especially 3D porous $Ni(OH)_2$/Ni capacitive electrodes.[29]

Herein, we fabricate binder-free integrated porous $Ni(OH)_2$/Ni film capacitive electrodes through a simple in-situ anode oxidation of 3D porous Ni film current collector which prepared by hydrogen bubble template electrochemical deposition. The 3D porous $Ni(OH)_2$/Ni electrodes demonstrate greatly higher specific

[a]*Shenzhen Institutes of Advanced Technology, Chinese Academy of Sciences, Shenzhen, P. R. China. E-mail: xz.fu@siat.ac.cn; rong.sun@siat.ac.cn; Fax: +86-755-86392299; Tel: +86-755-86392151*
[b]*Institute of Nano Science and Technology, University of Science and Technology of China, Suzhou 215123, P. R. China*
[c]*Department of Electronics Engineering, The Chinese University of Hong Kong, Hong Kong, China*
[d]*School of Materials Science and Engineering, Georgia Institute of Technology, Atlanta, GA 30332, United States*

capacitance of 828 mF/cm^2 than that of smooth Ni(OH)$_2$/Ni electrode (126 mF/cm^2). And the 3D porous Ni(OH)$_2$/Ni electrodes also exhibit outstanding capacitance retention of 95% after 1000 charge-discharge cycles at a current density of 10 mA/cm^2.

Experimental

Preparation of 3D porous Ni film current collectors

The 3D porous Ni films were prepared by a hydrogen bubble template electrochemical deposition.[23] All the reagents were analytical grade and were used without further purification, and all solutions were prepared with secondary deionized (DI) water. Nickel foil was cleaned five minutes with 1 M HCl, ethanol and DI water. Then it was used as the cathode for porous Ni film deposition, and a large area of nickel foil was processed as above as the anode. The distance between cathode and anode was kept at 2 cm. Porous Ni was deposited on the surface of the Ni substrate under a constant current density of 5 A/cm^2 for 60 s by using DC power PSW80-13.5 with electrolyte consisting of 0.2 M $NiCl_2$ and 2 M NH_4Cl at room temperature. After the electrochemical deposition, the porous Ni was thoroughly rinsed with DI water in order to remove the electrolyte solution from inside the pores for five times, dried first with an airflow and then in a vacuum oven at 50 ^oC for 5 h.

Preparation of 3D porous Ni(OH)$_2$/Ni integrated electrodes

A three-electrode cell was used in preparing the porous Ni(OH)$_2$/Ni film, containing the as-prepared porous Ni film or smooth Ni foil with 1cm×1cm surface area as the working electrode, a large area platinum foil as the counter electrode, and a Hg/HgO electrode as the reference electrode. Potentials were reported with respect to the Hg/HgO reference electrode. The electrochemical deposition experiments were performed in a freshly prepared 1 M KOH solution under quiescent conditions by a ZahnerZennium electrochemical workstation (Germany). Electrochemical anode oxidation of porous Ni to in-situ form outside Ni(OH)$_2$ thin layer was carried out potential dynamic method by subjecting the working electrode to potential cycling in the potential range of -0.1 V – 0.6 V at a scan rate of 25 mVs^{-1} for 50 cycles. Then the films were rinsed with DI water in order to remove the electrolyte solution for five times and then dried with airflow for morphology and electrochemical characterization. The Ni(OH)$_2$ film formed on the porous Ni film was called 3D porous Ni(OH)$_2$/Ni, and Ni(OH)$_2$ film formed on the smooth Ni foil was named smooth Ni(OH)$_2$/Ni.

Characterization and electrochemical measurement

The crystalline phase of samples were characterized by X-ray powder diffraction (XRD) using a Rigaku X-ray Diffractometer with Cu-Ka (1.5418 Å) radiation from 10 to 90° at a scanning speed of 5° min^{-1} operating at 30 kV and 20 mA. The morphology was observed using a Field Emission Scanning Electron Microscopy (FESEM, Nova NanoSEM 450). XPS analysis was recorder on a PHI 5800 XPS system, where Al Kα excitation source was used.

Before electrochemical measurements were performed, all samples were immersed in 6 M KOH solution for 5 h. Electrochemical measurements were carried out with a ZahnerZennium electrochemical workstation (Germany) using the conventional three-electrode electrochemical cell with 6 M KOH solution as electrolyte at room temperature. The as-prepared electrode was used as the working electrode, the potential was referred to a Hg/HgO reference electrode and a large area platinum foil was set as the counter electrode.

Cyclic voltammetry was conducted on each sample at various scan rates over a range of 0.01–0.1Vs^{-1} in a potential range of 0–0.5 V. Galvanostatic charge–discharge experiments were carried out at different current densities from 1 mA/cm^{2}to 10 mA/cm^2. The charge–discharge cycle performance was examined at a current density of 10 mA/cm^2 for 1000 cycles.

Results and discussion

Fig. 1 illustrates the fabrication process of 3D porous Ni film current collector by a hydrogen bubble template electrochemical deposition. As a large current density of 5 A/cm^2 is applied on the cathode of Ni substrate, numerous H_2 bubbles would be generated on the cathode substrate for the water electrolysis. At the same time, the Ni^{2+} ions in the electrolyte would be also electrochemically reduced and deposited on the cathode substrate. The deposited metal Ni atoms can only grow between H_2 bubbles then build 3D porous three-dimensional metal skeleton connected to the Ni substrate as the electrochemical reaction progress.

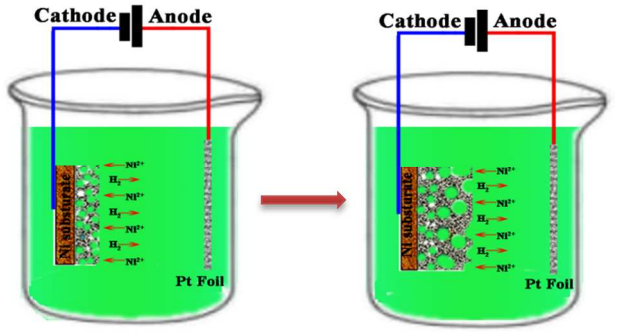

Fig. 1 Schematics illustrating the fabrication process of 3D porous Ni film current collector by hydrogen bubble template electrochemical deposition

Fig. 2 presents the typical XRD patterns of the porous Ni film and porous Ni(OH)$_2$/Ni film. There are strong diffraction peaks of porous Ni film at 2θ = 44°, 52°, 76°, which are in good agreement with the values from the standard card (JCPDS No.04-0850) of Ni metal. Except the strong Ni metal diffraction peaks, some new weak diffraction peaks appear at 2θ=19.2°、33°、38.5°、59°, 62.7° for porous Ni(OH)$_2$/Ni film. These new weak peaks are indexed to Ni(OH)$_2$ (JCPDS No.14-0117), confirming the formation of Ni(OH)$_2$ by anode oxidation of Ni substrate in the KOH solution. Ni is an active metal, which can be in-situ electrochemically oxidized to form Ni(OH)$_2$ outside coating layer in alkaline solution according to the previous report.[30] In addition, the low intensity of Ni(OH)$_2$ peaks relative to the remained Ni metal peaks indicate that the Ni(OH)$_2$

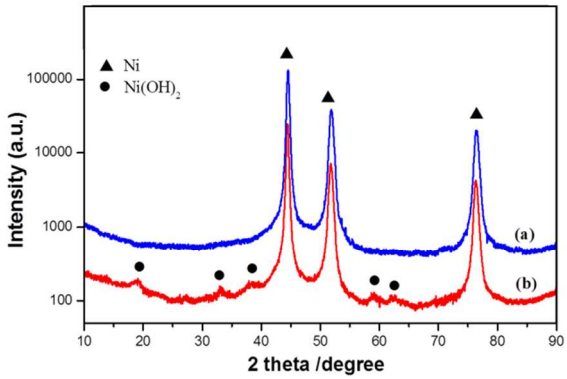

Fig. 2 XRD patterns of (a) 3D porous Ni films and (b) 3D porous Ni(OH)$_2$/Ni films.

layer is very thin on the surfaces of the porous nickel substrates.[31] To investigate the surface Ni sate of the electrodeposited 3D porous $Ni(OH)_2$/Ni film, the XPS analysis is performed, and measured results are shown in Fig.3. The typical $Ni2p_{3/2}$ and $2p_{1/2}$ peaks of 3D porous $Ni(OH)_2$/Ni film with two shake-up satellites (denoted as "sat.") are obtained at 873.9 eV and 856.3 eV, respectively (Fig. 3a). The spin-energy separation of 17.6 eV indicates characteristic of the $Ni(OH)_2$ phase, and in good agreement with previously reported[32, 33] The peak at 531.7 eV that are assigned to O1s photoelectrons (Fig. 3b), consisting of two oxygen bonds (533.4 eV and 531.6 eV), which can be associated with physi- and chemi- absorbed molecular water and $Ni(OH)_2$. This result is also in consistent with the XRD analysis, confirming the in-situ formation of $Ni(OH)_2$ capacitive materials on the 3D porous Ni skeleton.

Fig. 4 shows the SEM images of the as-prepared Ni-based film electrodes. Comparing the smooth Ni film substrate (Fig. 4a), the gray villous morphology is retained and more or less evenly coat on the surface of Ni film after formation of $Ni(OH)_2$ thin layer (Fig.4 b, c). SEM images in Fig. 4(d-f) clearly illustrate the as-prepared porous Ni film with 3D highly hierarchical porous network structure composed of numerous interconnected particles and interspaces. It can be observed in the large magnification SEM images (Fig. 4e, f)

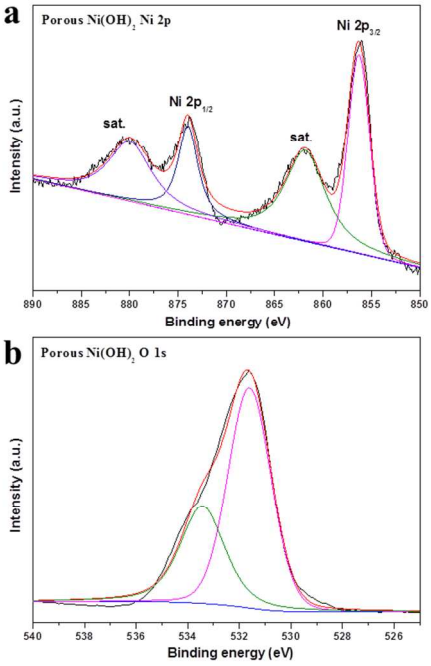

Fig. 3 (a) XPS peaks of Ni 2p of the 3D porous $Ni(OH)_2$/Ni film electrode, and (b) XPS peaks of O 1s of the 3D porous $Ni(OH)_2$/Ni film electrode.

that there are lots of interconnected small pores and gaps in the surface and the large pore walls. The pore size of large pores is mainly in the range from 5 to 20 μm, whereas the small pores/gaps are usually less than 1 μm even 100 nm. After electrochemical deposited, the 3D porous structure is well maintained and shows no obvious change comparing to the original 3D porous Ni films as shown in Fig. 4(g-i). It suggests the in-situ formed $Ni(OH)_2$ layer uniformly on the porous Ni scaffold. Comparing to the previous reported works about commercial low porous Ni foam due to large pore size (even more than 300 μm) and smooth wall for support $Ni(OH)_2$ capacitive thin film,[5-7] the as prepared Ni

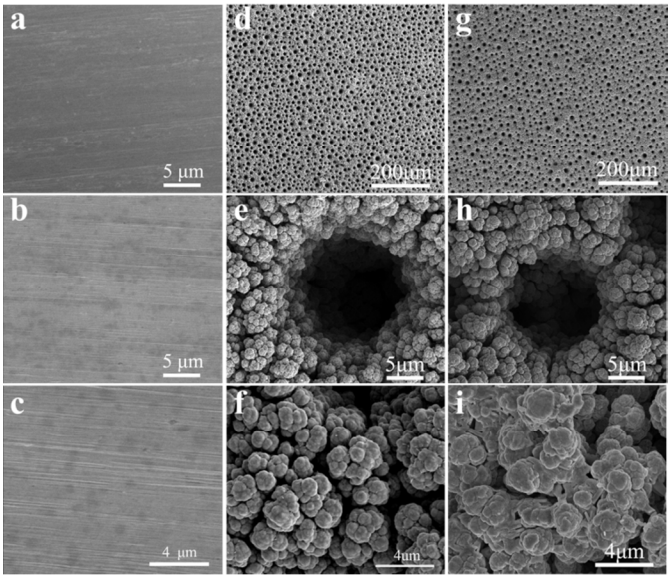

Fig.4 SEM images of (a) smooth Ni substrate, (b and c) smooth $Ni(OH)_2$ /Ni films, (d-f) 3D porous Ni films and (g-i) 3D porous $Ni(OH)_2$/Ni films.

current collector skeleton with 3D highly and hierarchically porous architecture would be expected to exhibit excellent electrochemical performance due to the high surface area and open porous structure for easily electrolyte penetration/diffusion as well highly porous interconnected Ni metallic network for fast electron conduction.[34] In addition, the $Ni(OH)_2$ active material is in-situ formed by anode oxidation of thin layer of outer 3D highly porous nickel skeleton itself while not obtained by deposition on Ni current collector, which might have better adhesion and low resistance between the $Ni(OH)_2$ capacitive material and Ni current collector.

Fig. 5 presents the CV curves of the different Ni-based electrodes at the scan rate of 10 $mV \cdot s^{-1}$ in the potential range from 0 V to 0.5 V in 6 M KOH electrolyte. In the first case, a

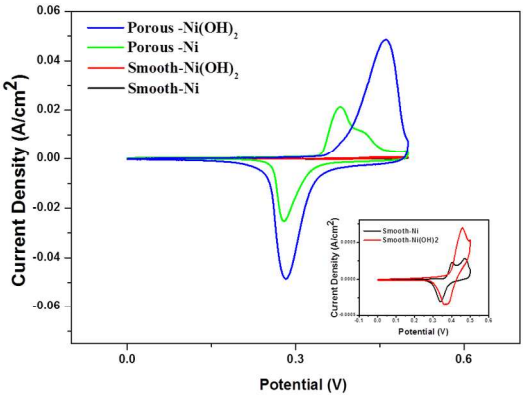

Fig. 5 Cyclic voltammograms of Ni-based electrodes recorded at 10 $mV \cdot s^{-1}$

pair of strong redox peaks is obviously observed for all the Ni-based electrodes. It is a typical pseudocapacitance faradaic redox behavior, which is very distinguished from the electric double layer capacitancethat normally close to an ideal rectangular shape of CV curve.[35] The redox peaks of the $Ni(OH)_2$ electrodes correspond to the conversion between

$Ni(OH)_2$ and NiOOH, which can be simply expressed as follows:[36]

$$Ni(OH)_2 + OH^- \Leftrightarrow NiOOH + H_2O + e^-$$

The anodic peak is due to the oxidation of $Ni(OH)_2$ to NiOOH, and the cathodic peak is for the reverse process.[23] The symmetric characteristic of anodic peak and cathodic peak reveals the excellent reversibility of the $Ni(OH)_2$electrodes. The porous Ni and smooth Ni electrodes also illustrate similar CV curves to that of $Ni(OH)_2$ since metallic Ni could be electrochemical oxidized to $Ni(OH)_2$ in KOH solution as the in situ preparation of $Ni(OH)_2$ layer on the porous Ni films. The 3D porous $Ni(OH)_2$/Ni electrodes demonstrate stronger current response in comparison with the porous Ni metallic film electrodes, implying that the pseudocapacitance mainly results from the $Ni(OH)_2$ film.[31] Moreover, the peak currents of the 3D porous $Ni(OH)_2$/Ni composite film electrodes are also much higher than that of the smooth $Ni(OH)_2$/Ni electrodes, indicating superior capacitance of the porous $Ni(OH)_2$/Ni electrodes due to the large area surface of $Ni(OH)_2$ on the porous Ni metallic film current collectors.

Fig. 6a shows the cyclic voltammograms (CV) of the 3D porous $Ni(OH)_2$/Ni composite film electrodes at scan rates from 10 to 100 $mV \cdot s^{-1}$ in the range between 0 and 0.5 V. Apparently, the shape of all the curves revealed that the capacitance mainly resulted from the pseudocapacitive capacitance. The shapes of CV curves are not significantly influenced by the increasing of the scan rates, indicating the improved mass transportation and electron conduction and the stable electrochemical capacitive behavior of the 3D porous $Ni(OH)_2$/Ni electrode. Moreover, the symmetry of two sets of redox peak reveals the good reversibility of the redox in the system. Furthermore, Fig. 6b shows the relation between oxidation/reduction peak current and the voltage scan rate of CV. The linear relationship between them reveals that the fast redox reaction of $Ni(OH)_2$ is controlled by surface absorption while not diffusion limitation.[24, 25] It also indicates that the as-prepared porous $Ni(OH)_2$ electrodes possess highly porous structure for electrolyte fast diffusion.

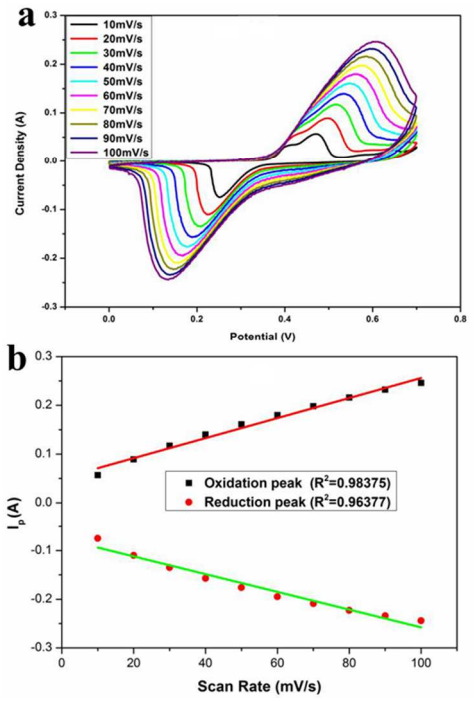

Fig. 6 (a) Cyclic voltammograms of 3D porous $Ni(OH)_2$/Ni film electrode obtained at various scan rates, and (b) the relationship between the peak current and scan rate.

Fig. 7 illustrates the constant current charge/discharge curves of the 3D porous $Ni(OH)_2$/Ni electrodes in 6 M KOH aqueous solution at various current densities within the potential window of 0 to 0.5 V. All the curves exhibit one couple of obvious charge and discharge plateaus, resulting from the transition between $Ni(OH)_2$ and NiOOH, indicating a typical pseudocapacitance behaviour, which is consistent with the results of CV test.[10] The specific capacitance can be calculated from the following equation:

$$C_s = \frac{I \cdot \Delta t}{\Delta V \cdot S}$$

Where C_s is the areal specific capacitance (F/cm^2) relative to the geometric area of capacitive electrodes, I is the discharge current (A), Δt is the discharge time (s), ΔV is the potential range during discharge (V), and S is the geometric area of the electrode. According to the equation, the specific capacitance of 3D porous $Ni(OH)_2$/Ni film electrode can be calculated based on the charge-discharge curves (Fig. 7a). The discharge specific capacitance values of the sample calculated from the discharge curves are 922, 889, 854, 835, 828 mF/cm^2 at the current density of 1,2,5,8 and 10 mA/cm^2, respectively. The variation of the specific capacitance with the current density is shown in Fig. 7b. As the current density increasing, the decrease in capacitance is owing to the limitation of the ion diffusion rate to satisfy the electronic neutralization during redox reaction and the inner active sites cannot sustain the redox transitions completely at higher current density.[26,27] The areal specific capacitance retention of the 3D porous $Ni(OH)_2$/Ni is 88% as the current density increasing from 1 mA/cm^2 to 10 mA/cm^2, indicating the 3D porous $Ni(OH)_2$/Ni electrodes possess good reversibility of electrochemical reaction even at high current density. The good rate capability of 3D porous $Ni(OH)_2$/Ni might result from

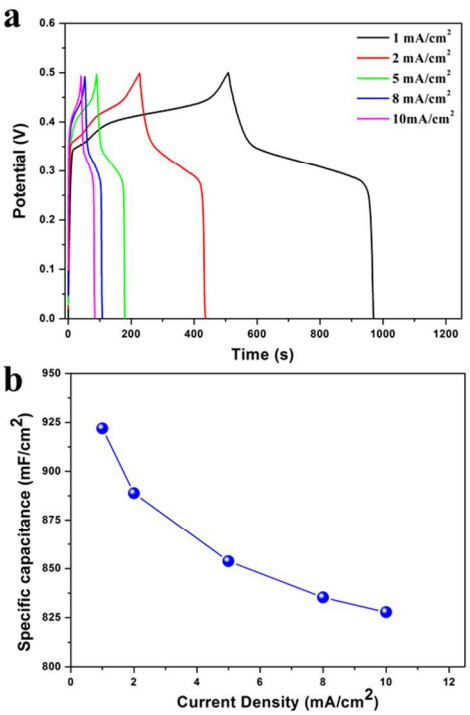

Fig. 7 (a) The constant charge and discharge curves of 3D porous $Ni(OH)_2$/Ni film electrodes at various current density, and (b) the relationship between the current density and discharge specific capacitance of 3D porous $Ni(OH)_2$/Ni film electrodes.

the highly porous structure for efficient electrolyte/ion diffusion and the effective micro-interconnected network for fast electron conduction.

To evaluate the long-term cyclic stability of 3D porous $Ni(OH)_2$/Ni film electrodes for electrochemical capacitors, galvanostatic charge/discharge measurements were carried out for 1000 cycles at the current density of 10 mA/cm^2. As shown in Fig. 8, the specific capacitance of the 3D porous $Ni(OH)_2$/Ni film electrode gradually decreases in initial 200 cycles, and henceforth tends to level off with the electrochemical cycling. Finally, approximately 5 % loss of specific capacitance after 1000 cycles indicates that the repetitive charge-discharges do not induce noticeable degradation of the 3D porous $Ni(OH)_2$/Ni film electrodes. All the 3D porous Ni, smooth $Ni(OH)_2$/Ni and Ni film electrodes demonstrate good cyclic stability, originating from the high redox reaction reversibility of $Ni(OH)_2$/NiOOH. The 3D porous $Ni(OH)_2$/Ni film electrodes exhibit greatly stable specific capacitance of about 828 mF/cm^2 than those of 3D porous Ni film electrodes (about 569 mF/cm^2), smooth $Ni(OH)_2$/Ni film electrodes (about 126 mF/cm^2) and smooth Ni foil electrodes (about 53 mF/cm^2) although the 3D porous structure does not improve the cycle stability. It also should be noted that the capacitance of porous Ni film, smooth $Ni(OH)_2$/Ni film, and smooth Ni foil electrodes increased with the continuous charge-discharge cycles in the staring stages. It might be originated from the metallic Ni current collector in-situ conversion to $Ni(OH)_2$ active materials in the electrochemical cycling.[37]

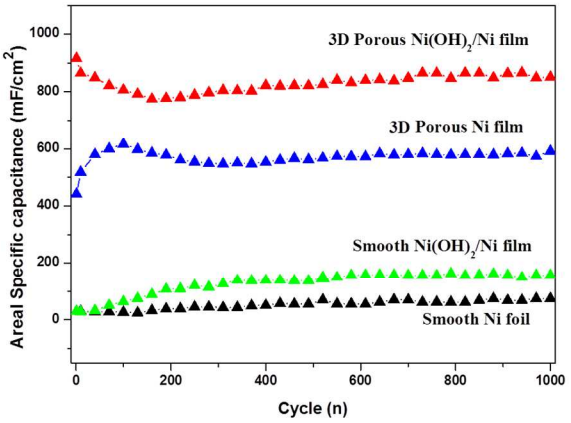

Fig. 8 Cycling performance of different electrodes at the current density of 10 mA/cm^2 after 1000 cycles.

The 3D network structure electrodes with high specific surface area and 3D conductive network scaffold to provide a highly conductive pathway for electrons and the catalyst of the conversion reaction to enhance the reverse reaction, meanwhile its interconnected porous network facilitate the rapid ion transport, shorten the solid-phase ion diffusion length to minimize the effect of sluggish solid-state ion transport and provide more electroactive sites for supercapacitor. The 3D porous structure plays a crucial role in optimizing superior capacitive performance of the $Ni(OH)_2$ film, which is a good candidate as an electrode material for electrochemical capacitor. Thus the 3D porous $Ni(OH)_2$/Ni film is a promising electrode for high performance supercapacitors.

Conclusions

3D porous $Ni(OH)_2$/Ni integrated film electrodes are fabricated by simple electrochemical methods of hydrogen bubble template electrodeposition then in-situ anode oxidation. The 3D porous $Ni(OH)_2$/Ni integrated film electrodes demonstrate greatly higher stable specific capacitance of 828 mF/cm^2 than that of smooth $Ni(OH)_2$/Ni film electrodes (about 126 mF/cm^2) at the current density of 10 mA/cm^2.The 3D porous $Ni(OH)_2$/Ni integrated film electrodes also exhibit excellent cyclic stability and rate capability. The high electrochemical capacitive performance of 3D porous $Ni(OH)_2$/Ni integrated film electrodes might result from the high surface area of $Ni(OH)_2$ layer in-situ directly formed on the highly porous interconnected conductive Ni current collectors.

Acknowledgements

This work was financially supported by National Natural Science Foundation of China (No.21203236, 21171015), Guangdong and Shenzhen Innovative Research Team Program (No.2011D052, KYPT20121228160843692), Shenzhen Electronic Packaging Materials Engineering Laboratory (2012-372), Shenzhen Electronic Packaging and Device Assembly Key Laboratory (ZDSYS20140509174237196), the "1000 plan" from Chinese Government, program for New Century Excellent Talents in University (NCET), Sofjakovalevskaja award from Alexander von Humboldt Foundation.

Notes and references

1. P. Simon and Y. Gogotsi, *Nat. Mater.*, 2008, **7**, 845-854.
2. A.S. Arico, P. Bruce, B. Scrosati, J.M. Tarascon and W. Van Schalkwijk, *Nat. Mater.*, 2005, **4**, 366-377.
3. M. Winter and R. J. Brodd, *Chem. Rev.*, 2004, **104**, 4245-4269.
4. C. Liu, F. Li, L.P. Ma and H.M. Cheng, *Adv. Mater.*, 2010, **22**, 28-62.
5. G. Wang, L. Zhang and J. Zhang, *Chem. Soc. Rev.*, 2012, **41**, 797-828.
6. G.W. Yang, C.L. Xu and H.L. Li, *Chem. Commun.*, 2008, 6537-6539.
7. Y. Zhang, H. Feng, X. Wu, L. Wang, A. Zhang, T. Xia, H. Dong, X. Li and L. Zhang, *Int. J. Hydrogen Energ.*, 2009, **34**, 4889-4899.
8. U.M. Patil, K.V. Gurav, V.J. Fulari, C.D. Lokhande and O.S. Joo, *J. Power Sources*, 2009, **188**, 338-342.
9. J. Li, F. Luo, X. Tian, Y. Lei, H. Yuan and D. Xiao, *J. Power Sources*, 2013, **243**, 721-727.
10. H. Jiang, T. Zhao, C. Li and J. Ma, *J. Mater. Chem.*, 2011, **21**, 3818-3823.
11. H. Wang, H.S. Casalongue, Y. Liang and H. Dai, *J. Am. Chem. Soc.*, 2010, **132**, 7472-7477.
12. F. Zhang, D. Zhu, X.A. Chen, X. Xu, Z. Yang, C. Zou, K. Yang and S. Huang, *Phys. Chem. Chem. Phys.*, 2014, **16**, 4186-4192.
13. G. Hu, C. Li and H. Gong, *J. Power Sources*, 2010, **195**, 6977-6981.
14. G. Zhang and X.W. Lou, *Adv. Mater.*, 2013, **25**, 976-979.
15. Z. Tang, C.H. Tang and H. Gong, *Adv. Funct. Mater.*, 2012, **22**, 1272-1278.
16. H. Chang, J. Kang, L. Chen, J. Wang, K. Ohmura, N. Chen, T. Fujita, H. Wu and M. Chen, *Nanoscale*, 2014, **6**, 5960-5966.
17. X.C. Dong, H. Xu, X.W. Wang, Y.X. Huang, M.B. Chan-Park, H. Zhang, L.H. Wang, W. Huang and P. Chen, *ACS Nano*, 2012, **6**, 3206-3213.
18. U. Singh, A. Banerjee, D. Mhamane, A. Suryawanshi, K.K. Upadhyay and S. Ogale, *RSC Adv.*, 2014, **4**, 39875-39883.
19. J.T. Zhang, S. Liu, G.L. Pan, G.R. Li and X.P. Gao, *J. Mater. Chem. A*, 2014, **2**, 1524-1529.

20. J. Ji, L. L. Zhang, H. Ji, Y. Li, X. Zhao, X. Bai, X. Fan, F. Zhang and R. S. Ruoff, *ACS Nano*, 2013, **7**, 6237-6243.
21. X. Chen, K. Sun, E. Zhang and N. Zhang, *RSC Adv.*, 2013, **3**, 432-437.
22. J. Xiao, S. Yang, L. Wan, F. Xiao and S. Wang, *J. Power Sources*, 2014, **245**, 1027-1034.
23. H.C. Shin, J. Dong, and M.L. Liu, Adv. Mater., 2003, **15**, 1610-1614.
24. J. Yan, W. Sun, T. Wei, Q. Zhang, Z. Fan and F. Wei, *J. Mater. Chem.*, 2012, **22**, 11494-11502.
25. X. Tian, C. Cheng, L. Qian, B. Zheng, H. Yuan, S. Xie, D. Xiao and M. M. F. Choi, *J. Mater. Chem.*, 2012, **22**, 8029-8035.
26. M.S. Wu and J.F. Wu, *J. Power Sources*, 2013, **240**, 397-403.
27. Y. Li, W.Z. Jia, Y.Y. Song and X.H. Xia, *Chem. Mater.*, 2007, **19**, 5758-5764.
28. Q.Q. Xiong, J.P. Tu, Y. Lu, J. Chen, Y.X. Yu, X.l. Wang and C.D. Gu, *J Mater. Chem.*, 2012, **22**, 18639-18645.
29. X.H. Xia, J. P. Tu, Y. Q. Zhang, Y. J. Mai, X. L. Wang, C.D. Gu and X.B. Zhao, *J. Phys. Chem. C*, 2011, **115**, 22662-22668.
30. Z. Wu, X.L. Huang, Z.L. Wang, J.J. Xu, H.G. Wang and X.B. Zhang, *Sci. Rep.*, 2014, **4**, 3669-3677.
31. D.S. Kong, J.M. Wang, H.B. Shao, J.Q. Zhang and C.N. Cao, *J. Alloy Compd.*, 2011, **509**, 5611-5616.
32. J. Yan, Z. Fan, W. Sun, G. Ning, T. Wei, Q. Zhang, R. Zhang, L. Zhi and F. Wei, *Adv.Funct. Mater.*, 2012, 22, 2632-2641.
33. J. W. Lee, T. Ahn, D.Soundararajan, J. M. Ko and J.D. Kim, *Chem. Commun.*, 2011, 47, 6305-6307.
34. X.H. Xia, J.P. Tu, Y. Q. Zhang, Y.J. Mai, X.L. Wang, C.D. Gu and X.B. Zhao, *J. Phys. Chem. C*, 2011, **115**, 22662-22668.
35. D.D. Zhao, S.J. Bao, W.H. Zhou and H.L. Li, *Electrochem. Commun.*, 2007, **9**, 869-874.
36. H. Du, L. Jiao, K. Cao, Y. Wang and H. Yuan, *ACS Appl. Mater. & Inter.*, 2013, **5**, 6643-6648.
37. W. Xing, S. Qiao, X. Wu, X. Gao, J. Zhou, S. Zhuo, S.B. Hartono and D. Hulicova-Jurcakova, *J. Power Sources*, 2011, **196**, 4123-4127.

